

Monitoring Spontaneous Charge-density Fluctuations by Single-molecule Diffraction of Quantum Light

Konstantin E. Dorfman*

*State Key Laboratory of Precision Spectroscopy,
East China Normal University, Shanghai 200062, China*

Shahaf Asban,[†] Lyuzhou Ye, Daeheum Cho, and Shaul Mukamel[‡]
*Department of Chemistry and Department of Physics and Astronomy,
University of California, Irvine, California 92697-2025, USA*

Jérémy R. Rouxel

*Laboratory of Ultrafast Spectroscopy, École Polytechnique
Fédérale de Lausanne, CH-1015 Lausanne, Switzerland and
SwissFEL, Paul Scherrer Institut, 5232 Villigen PSI, Switzerland*

(Dated: January 30, 2019)

Homodyne X-ray diffraction signals produced by classical light and classical detectors are given by the modulus square of the charge density in momentum space $|\sigma(\mathbf{q})|^2$, missing its phase which is required in order to invert the signal to real space. We show that quantum detection of the radiation field yields a linear diffraction pattern that reveals $\sigma(\mathbf{q})$ itself, including the phase. We further show that repeated diffraction measurements with variable delays constitute a novel multidimensional measure of spontaneous charge-density fluctuations. Classical diffraction, in contrast, only reveals a subclass of even-order correlation functions. Simulations of two dimensional signals obtained by two diffraction events are presented for the amino acid cysteine.

I. INTRODUCTION

Photon counting, as described by the quantum theory of detection, is associated with annihilation of a radiation mode [1]. Any detectable change in the number of photons requires at least two light-matter interactions. Diffraction of a classical source on quantum matter is thus a second order process in the light/matter interaction. Sources with a low photon flux [2–8] or short wavelength [9–13] - that can detect $(\Delta n)\hbar\omega$ is detectable (Δn being the change in photon number) - now exist. Taking the quantum nature of light into account is now called for.

Multidimensional diffraction can be measured by photon coincidence counting obtained by

subjecting the molecule to sequences of pulses. The underlying matter information is given by the multi-point correlation functions of the charge density which governs the spontaneous charge fluctuations. The response and spontaneous fluctuations of both field and charge density are mixed due to their quantum nature and classical response theory, which is causal does not apply [14]. Thus, multidimensional spectroscopy, which involves several perturbations followed by a single measurement is fundamentally different from multidimensional diffraction, which consists of a series of measurements, and thus may not be retrieved simply by data processing of classical signals. Multidimensional diffraction carries new type of information related to spontaneous charge fluctuations, which is not accessible by classical light [15].

In this letter we consider off-resonant diffraction of nonclassical X-ray sources, and explore phase dependent quantum corrections to diffraction, involving a *single* light-matter in-

* Email: dorfman@lps.ecnu.edu.cn

[†] sasban@uci.edu

[‡] smukamel@uci.edu

teraction. Photons are not generated in this order (this requires two interactions), which only causes phase change of the field. This results in a detectable photon intensity diffraction pattern when coupled to local quantum fluctuations at the detector. We denote this process as linear quantum diffraction (LQD) (i.e linear in the charge density).

We consider an incoming light prepared either in a coherent state or in a Fock state interacting with a local field mode which is eventually detected by photon annihilation in the detected mode [1]. Field intensity measurements show that local quantum fluctuations at the detector coupled to the detected mode generate signal linear in the charge density. Coherent (classical-like) or single-photon states provide higher degrees of spatial and spectral resolution, whereas an N -photon Fock state yields lower resolution.

Crystallographic signals generated by classical light are quadratic in the charge density in momentum space $\sigma(\mathbf{q})$. The phase is not available and phase reconstruction algorithms [16, 17] or heterodyne detection [18] are required to retrieve the real-space charge density $\sigma(\mathbf{r}) = \int d\mathbf{q} e^{i\mathbf{q}\cdot\mathbf{r}} \sigma(\mathbf{q})$. Heterodyne detection of the signal field is achieved by interference with a Local Oscillator (LO) [19], which must be varied for each scattering angle. Phase reconstruction algorithms usually require a reasonable initial guess in order to converge to the correct structure [20, 21]. Signals linear in the charge density, can reveal the phase of the Fourier-transformed charge densities and the crystallographic image. Thus quantum detected diffraction offers an interesting possibility for overcoming the phase problem without scanning the LO for each detection angle. Furthermore, classical diffraction can be viewed as an ensemble average of different trajectories. Each detection event results from a trajectory terminated in a point at the detector. It is further blurred by the detector response function, even for infinitesimal detection area (pixel size). Using quantum detection, this response can be studied at the single trajectory level, enhancing the resolution by reducing the spread and minimizing the noise [22].

Repeated measurements involving sequences of n delayed pulses result in multiple diffraction signals each linear in the charge density given by n -dimensional correlation functions of the charge density. A classical diffraction experiment, in contrast, only reveals even order correlation functions [23]. Since the phase of the charge density in momentum-space corresponds to translation in real-space, correlation functions such as $\langle \sigma(\mathbf{q}_1, t_1) \sigma(\mathbf{q}_2, t_2) \rangle$ carry interesting structural-dynamical information that is inaccessible with classical light.

II. THE LQD SIGNAL

Off-resonant diffraction is described by the minimal coupling matter/field interaction Hamiltonian [24, 25], $\mathcal{H}_I = \int d\mathbf{r} \sigma(\mathbf{r}, t) \mathbf{A}^2(\mathbf{r}, t)$ where σ is the charge-density operator, while \mathbf{A} is the vector potential. We first assume that the incoming light pulse is described by a multi-mode coherent state $|\psi_p(0)\rangle = \prod_{\mathbf{p}, \lambda} |\alpha_{\mathbf{p}, \lambda}\rangle$. Here $\alpha_{\mathbf{p}, \lambda}$ represents the amplitude of coherent state of a mode with momentum \mathbf{p} and polarization λ . The diffraction pattern is obtained from the time-integrated spatially-gated intensity at point \mathbf{r} of the detector. Assuming no temporal gate $\tilde{F}_t^I(\tilde{t}, \omega) = 2\pi\delta(\omega)$ and performing rotational averaging $\langle \hat{\mathbf{r}}_m \hat{\mathbf{r}}_n \rangle = \delta_{m,n}/3$, the first order expansion of the signal in Eq. (A1) assumes the form

$$S_m^{(1)}[\mathbf{q}_{\{\mathbf{k}\}}(\mathbf{r})] \propto \Re \sum_{\mathbf{k}, \mathbf{k}_p} \omega_{\mathbf{k}} \mathcal{E}_m^*(\mathbf{k}) \mathcal{A}_m(\mathbf{k}_p) \times \langle \sigma[\mathbf{q}_{\{\mathbf{k}\}}(\mathbf{r}), \omega_{\mathbf{q}}] \rangle e^{-i\mathbf{q}_{\{\mathbf{k}\}}(\mathbf{r}) \cdot \mathbf{r}} \quad (1)$$

$$(2)$$

where m is a cartesian component of the field, $\mathbf{q}_{\{\mathbf{k}\}}(\mathbf{r}) = \mathbf{k}_p - k\hat{\mathbf{r}}$ and $\omega_{\mathbf{q}} = \omega_{\mathbf{k}_p} - \omega_{\mathbf{k}}$ are the diffraction wavevector at a corresponding frequency, $\hat{\mathbf{r}}$ is a unit vector in the detection direction; the field and the vector potential amplitudes $\mathcal{E}_m(\mathbf{k})$ and $\mathcal{A}_n(\mathbf{k}_p)$ are given by expectation values of the corresponding operators (see Eqs. (A6) and (A7)). The signal Eq. (1), which depends on the momentum \mathbf{k} , is governed by the initial state configuration, polarization and

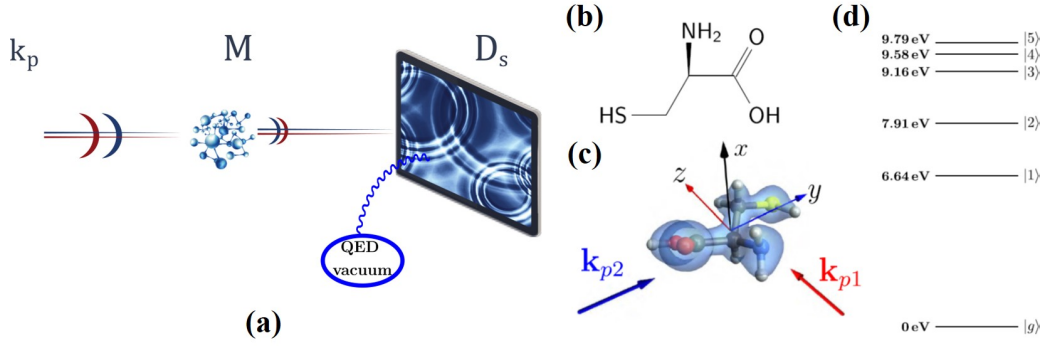


FIG. 1. (a) The LQD setup: single photon with momentum \mathbf{k}_p diffracted off a single molecule and the LQD is detected on a screen (preparation pulse is not depicted). The blue circle represents the quantum vacuum fluctuations of QED that interacts once with the detector in the LQD scheme. (b) The chemical structure of cysteine. (c) The orientated cysteine and the ground state charge density σ_{gg} . The pulse configuration: $\mathbf{k}_{p1} \parallel \hat{z}$ and $\mathbf{k}_{p2} \parallel \hat{y}$. (d) Energy levels of the ground (g) and valence excited ($e = 1, 2, \dots, 5$) states.

other degrees of freedom. The spatial resolution is controlled by the the diffraction wvector $\mathbf{q}_{\{\mathbf{k}\}}(\mathbf{r})$; $\omega_{\mathbf{q}}$ can be a useful tool for monitoring transient states of the charge density. A similar result is obtained for a single-photon Fock state $|\psi_{1F}(0)\rangle = \sum_{\mathbf{p},\lambda} \Phi_{\mathbf{p},\lambda} |1_{\mathbf{p},\lambda}\rangle$ (see Appendix A), where $\Phi_{\mathbf{p},\lambda}$ represents the Fock state amplitude.

Time-resolved LQD. In this setup, an actinic pulse initially prepares the molecule in a superposition of electronic states and the LQD performed after a delay T probes the excited state dynamics. The superposition of electronic states is described by density matrix elements $\rho_{ab}^{(0)}$ with the phase $e^{i\phi_{ab}}$, where a and b are molecular electronic eigenstates. The impulsive diffraction off this state after time delay T is governed by the transition charge density element $\sigma_{ab} = \langle a | \hat{\sigma} | b \rangle$. The sum-over-states expression of Eq. (1) for a coherent or single photon state the reads

$$S_m^{(1)}[\mathbf{q}(\mathbf{r}), T] \propto \Re \mathfrak{e} \sum_{\mathbf{k}, \mathbf{k}_p} \sum_{a,b} \omega_{\mathbf{k}} \mathcal{E}_m^*(\mathbf{k}) \mathcal{A}_m(\mathbf{k}_p) \times \text{Tr} \left\{ \sigma_{ab}[\mathbf{q}(\mathbf{r}), \omega_{\mathbf{q}}] \rho_{ab}^{(0)} \right\} e^{-i\mathbf{q}(\mathbf{r}) \cdot \mathbf{r} + i\phi_{ab}}. \quad (3)$$

Thus, the LQD signal may reveal the single molecule coherence and its phase as well as the

transient charge density and its phase.

We now turn to a different state of the incoming field: an N -photon Fock state described by the wavefunction $|\psi_{NF}(0)\rangle = \sum_{\mathbf{p},\lambda} \Phi_{\mathbf{p},\lambda}^{(N)} |N_{\mathbf{p},\lambda}\rangle$ where $\Phi_{\mathbf{p},\lambda}^{(N)}$ is the N -photon amplitude of the \mathbf{p} mode with polarization λ . Assuming no temporal gating we obtain from Eq. (A1) upon orientational averaging,

$$S_m^{(1)}[\mathbf{q}(\mathbf{r})] \propto \Re \mathfrak{e} \sum_{\mathbf{k}_p, \lambda} \mathcal{E}_{m\lambda}^*(\mathbf{k}_p) \mathcal{A}_{m\lambda}(\mathbf{k}_p) \times \langle \sigma[\mathbf{q}(\mathbf{r}), 0] \rangle e^{-i\mathbf{q}(\mathbf{r}) \cdot \mathbf{r}}, \quad (4)$$

where the abbreviated wvector $\mathbf{q}(\mathbf{r}) \equiv \mathbf{q}_{\{\mathbf{k}\}}(\mathbf{r}) = \mathbf{k}_p - k_p \hat{\mathbf{r}}$ and $\mathcal{A}_{m\lambda}(\mathbf{k}_p)$ are defined in Eqs. (A9) and (A10), respectively. Note that, unlike the coherent or the single photon initial states, the N -photon Fock state signal depends solely on the pump momentum and carries no temporal information, since the frequency argument in the charge density is zero. This can be explained as follows: The N -photon Fock state has a fixed number of photons in each mode. Thus, annihilation and consequent creation of the photon must occur in the same mode to conserve the photon number. In contrast, annihilation of the photon in the single-photon Fock state yields the vacuum state. Thus,

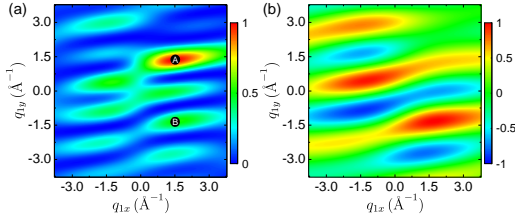


FIG. 2. (a) Classical homodyne and (b) first order linear quantum diffraction \mathbf{q}_1 scattering pattern in the $q_{1z} = 1.89 \text{ \AA}^{-1}$ plane. The first pulse \mathbf{k}_{p1} propagates along z . Points A and B were used in the calculated diffraction signals.

the diffracted photon created from the vacuum may have a different momentum. The coherent source has a well-defined average photon number, rather than a fixed photon number, which allows diffraction into a mode other than the pump. Similarly the time-resolved equivalent of Eq. (4) yields

$$S_m^{(1)}[\mathbf{q}(\mathbf{r}), T] \propto \Re \epsilon \sum_{\mathbf{k}_p, \lambda} \sum_{a, b} \mathcal{E}_{m\lambda}^*(\mathbf{k}_p) \mathcal{A}_{m\lambda}(\mathbf{k}_p) \times \text{Tr} \left\{ \sigma_{ab}[\mathbf{q}(\mathbf{r}), 0], 0 \right\} \rho_{ab}^{(0)}(T) \left\} e^{-i\mathbf{q}(\mathbf{r}) \cdot \mathbf{r} + i\phi_{ab}}. \quad (5)$$

Heterodyne detection with a classical local oscillator field measures the interference of a non-interacting local oscillator with interacting beam (see Eq. (B1)). The role of the local oscillator is then played by vacuum field fluctuations, which couple to modes scattered off the matter.

III. MULTIDIMENSIONAL QUANTUM DIFFRACTION

Spontaneous fluctuations of any physical quantity are described by its multi-point correlation functions. In the case of the charge density these are $\langle \sigma(\mathbf{q}_1, T_1) \sigma(\mathbf{q}_2, T_2) \dots \rangle$. We now show how these can be measured by a series of quantum diffraction processes. We consider a single molecule undergoing a sequence of [26] n quantum diffraction events. The

pulses can have arbitrary spectral and temporal profiles, provided they are temporally well-separated and tuned far from any material resonance. An n -th order coincidence counting of LQD photons at positions $(\mathbf{r}_1, \mathbf{r}_2, \dots, \mathbf{r}_n)$ is generated by multiple incoming single photon pulses with momenta $(\mathbf{k}_{p1}, \mathbf{k}_{p2}, \dots, \mathbf{k}_{pn})$ and delays (T_1, T_2, \dots, T_n) .

$$S_q^{(n)}(\mathbf{q}_1, T_1; \dots; \mathbf{q}_n, T_n) \propto \mathcal{E}_1 \dots \mathcal{E}_n \times \langle \langle \mathcal{T} \bar{\sigma}(\mathbf{q}_1, T_1) \dots \bar{\sigma}(\mathbf{q}_n, T_n) \rangle \rangle, \quad (6)$$

where $\bar{\sigma} = \sigma + \sigma^\dagger$, and the first momentum transfer is $\mathbf{q}_1 = \mathbf{k}_{p1} - \mathbf{k}_1$, followed by $\mathbf{q}_2 = \mathbf{k}_{p2} - \mathbf{k}_2$, etc, with \mathbf{k}_n being the wavevector of the scattered photon.

We now examine the two lowest-order signals. In the simplest (2D) experiment, the molecule is subjected to two off-resonant pulses, with wavevectors \mathbf{k}_{p1} and \mathbf{k}_{p2} . A scattered single-photon amplitude from pulse 1 with frequency ω_1 is contracted with the incoming photon amplitude, and the resulting photon is collected in the direction \mathbf{k}_1 at time T_1 . The molecule is in a superposition state during the interpulse delay, after which the second pulse is scattered, and the photon amplitude is contracted with the incoming photon amplitude such that the resulting photon with frequency ω_2 is collected in the \mathbf{k}_2 direction at time T_2 .

In the impulsive limit, the 2D signal can be written as (see Fig. 5 and discussion therein)

$$S^{(2)}(\mathbf{q}_1, T_1; \mathbf{q}_2, T_2) \propto \langle \bar{\sigma}(\mathbf{q}_2, T_2) \bar{\sigma}(\mathbf{q}_1, T_1) \rangle. \quad (7)$$

Higher-order signals can be calculated similarly.

We have simulated the 2D diffraction signals Eq.(7) from a single oriented cysteine molecule (see Fig.1(b) and (c)). Quantum chemistry calculations were performed by using the MOLPRO code [27]. The optimized geometry was obtained at the Hartree-Fock/cc-pVDZ [28] level of theory. The lowest six valence electronic energy levels were calculated at the CASSCF(6/6)/cc-pVDZ level of theory [29–31] are depicted in Fig.1(d). The transition density matrix was evaluated using

$$\sigma_{ij}(\mathbf{r}) = \sum_{mn} T_{mn}^{(ij)} \phi_m(\mathbf{r}) \phi_n(\mathbf{r}). \quad (8)$$

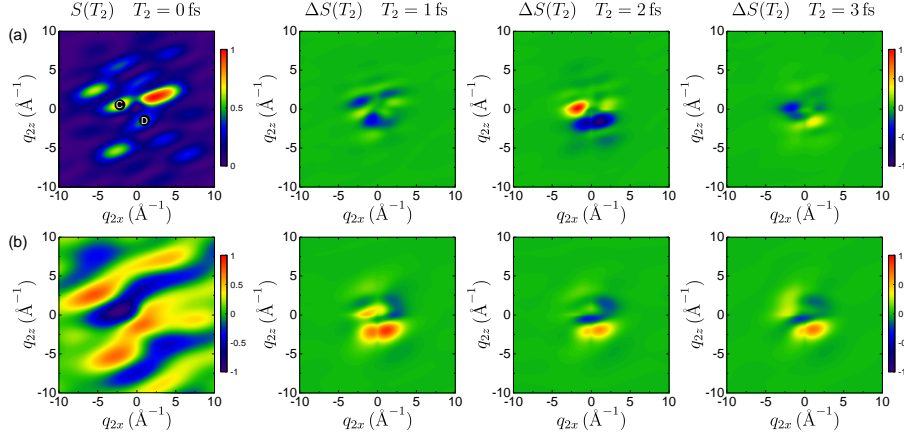


FIG. 3. The \mathbf{q}_2 diffraction patterns at the given \mathbf{q}_1 point A for (a) classical homodyne $S_c^{(4)}(\mathbf{q}_1, T_1 = 0; \mathbf{q}_2, T_2)$ and (b) second order linear quantum diffraction $S_q^{(2)}(\mathbf{q}_1, T_1 = 0; \mathbf{q}_2, T_2)$ signals at four time delays T_2 in the $q_{2y} = 1.89 \text{ \AA}^{-1}$ plane. The second pulse \mathbf{k}_{p2} propagates along y . To highlight the changes, in columns 2, 3, and 4, we plot the signal difference $\Delta S(T_2) = S(T_2) - S(T_2 = 0)$.

Here, the indices i, j run over the valence eigenstates. $T_{mn}^{(ij)}$ is the transition density-matrix element between states i and j for the m and n atomic orbitals.

We consider diffraction signals from the ground state (g). In the impulsive limit, the classical homodyne signal for single pulse scattering is given by the sum-over-states expression Eq. (B5) which determines the (transition) charge density $\sigma_{ag}(\mathbf{q}_1)$ between two electronic states a and g in momentum $\mathbf{q}_1 \equiv \mathbf{k}_1 - \mathbf{k}_{p1}$ space. The homodyne detected signal Eq. (B5) misses the phase of $\sigma_{ag}(\mathbf{q}_1)$.

The linear (1D) quantum diffraction signal solely gives the ground state charge density:

$$S_q^{(1)}(\mathbf{q}_1, T_1) \propto \langle \bar{\sigma}(\mathbf{q}_1, T_1) \rangle = 2\Re\epsilon[\sigma_{gg}(\mathbf{q}_1, T_1)]. \quad (9)$$

Both signals Eqs. (B5) and (9) are independent on the time delay T_1 . Time-dependent signals can be obtained by first preparing the molecule in a superposition state [18, 23]. The first pulse \mathbf{k}_{p1} propagates along z , while the \mathbf{q}_1 diffraction signals $S_c^{(2)}(\mathbf{q}_1)$ and $S_q^{(1)}(\mathbf{q}_1)$ are detected in the (q_{1x}, q_{1y}) plane; see Fig. 2. The scattering shows rich pattern in \mathbf{q}_1 space. The ho-

modyne detected signal (Fig. 2(a)) is positive, and several peaks can be observed in the \mathbf{q}_1 domain. The linear quantum diffraction signal may be negative. The classical $S_c^{(2)}$ signal (Eq. (B5)) is expressed as the modulus square form of (transition) charge densities in momentum space. The quantum $S_q^{(1)}$ signal (Eq. (9)) in contrast depends on both the amplitude and phase of charge densities, making it possible to extract the real space ground state charge density $\sigma_{gg}(\mathbf{r})$.

To study the charge density dynamical fluctuations, we resort to the $S_q^{(2)}$ signal. To investigate the two-photon coincidence scattering pattern in \mathbf{q}_2 space, we select the \mathbf{q}_1 point A = $(1.51 \text{ \AA}^{-1}, 1.36 \text{ \AA}^{-1})$ in Fig. 2(a). The classical homodyne signal for \mathbf{q}_2 scattering is given by Eq. (B7). The second order LQD signal is

$$\begin{aligned} S_q^{(2)}(\mathbf{q}_1, T_1 = 0; \mathbf{q}_2, T_2) &\propto \langle \bar{\sigma}(\mathbf{q}_2, T_2) \bar{\sigma}(\mathbf{q}_1, 0) \rangle \\ &= \sum_a [\sigma_{ga}(\mathbf{q}_2) + \sigma_{ag}^*(\mathbf{q}_2)] [\sigma_{ag}(\mathbf{q}_1) + \sigma_{ga}^*(\mathbf{q}_1)] e^{-i\omega_{ag}T_2}. \end{aligned} \quad (10)$$

Because the molecule is initially in the ground state, the signal depends only on the second time delay T_2 .

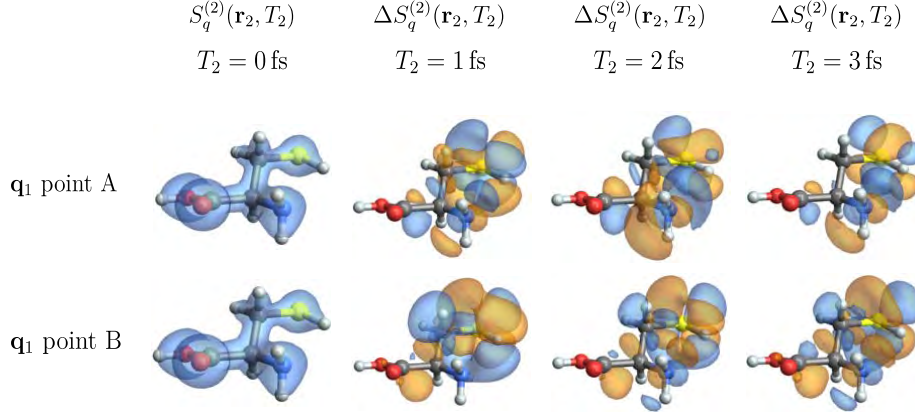


FIG. 4. The time-dependent charge density obtained using Eq. (11) for \mathbf{q}_1 points A = $(1.51 \text{ \AA}^{-1}, 1.36 \text{ \AA}^{-1})$ and B = $(1.51 \text{ \AA}^{-1}, -1.36 \text{ \AA}^{-1})$ marked in Fig. 2. We show the full signal at $T_2 = 0 \text{ fs}$, and the signal differences $\Delta S_q^{(2)}(\mathbf{r}_2, T_2) = S_q^{(2)}(\mathbf{q}_1, T_1 = 0; \mathbf{r}_2, T_2) - S_q^{(2)}(\mathbf{q}_1, T_1 = 0; \mathbf{r}_2, T_2 = 0)$ for other plots.

Figure 3 depicts the \mathbf{q}_2 scattering pattern in the $q_{2y} = 1.89 \text{ \AA}^{-1}$ plane, where the second pulse \mathbf{k}_{p2} propagates along y . The first column shows the signals at $T_2 = 0$. Again, we see that the classical $S_c^{(4)}$ signal (Fig. 3(a)) is always positive, while the quantum signal $S_q^{(2)}$ (Fig. 3(b)) may be negative. Since signal is dominated by the time-independent pathways, *i.e.*, $c = d$ in Eq. (B7) and $a = g$ in Eq. (10), the diffraction signals at different time delays look very similar. To better visualize the changes, we plot the signal difference $S(T_2) - S(T_2 = 0)$ in columns 2, 3, and 4, where the time-independent background has been subtracted. Rich temporal patterns in \mathbf{q}_2 originates from interferences between the various scattering pathways. By Fourier transform of the time-domain signal into the frequency (Ω) domain, we can identify the electronic coherences that contribute to the dynamics of the signal. If Fig. 6 of the SI we display such spectra at the points C and D of Fig. 3.

The classical $S_c^{(2)}$ signal represents the electron density fluctuations in momentum space, and may be used to image the real-space charge-density correlation functions. The quantum phase-dependent $S_q^{(2)}$ signal, in contrast, can retrieve the time-dependent transition charge densities in real space. Fourier transformation

of the second order LQD signal Eq. (10) into real space \mathbf{r}_2 at a given \mathbf{q}_1 point in Fig. 2 gives

$$\begin{aligned}
 & S_q^{(2)}(\mathbf{q}_1, T_1 = 0; \mathbf{r}_2, T_2) \\
 & \propto \int d\mathbf{q}_2 e^{i\mathbf{q}_2 \cdot \mathbf{r}_2} S_q^{(2)}(\mathbf{q}_1, T_1 = 0; \mathbf{q}_2, T_2) \\
 & = 2 \sum_a [\sigma_{ag}(\mathbf{q}_1) + \sigma_{ga}^*(\mathbf{q}_1)] e^{-i\omega_{ag} T_2} \sigma_{ga}(\mathbf{r}_2).
 \end{aligned} \tag{11}$$

Figure 4 depicts the real-space signal at the two \mathbf{q}_1 points A and B marked in Fig. 2 for different time delays T_2 . At $T_2 = 0 \text{ fs}$, the signal looks similar to the ground state charge density (see Fig. 1 (c)), because the $\sigma_{gg}(\mathbf{r}_2)$ term dominates Eq. (4). As in Fig. 3 the other plots at $T_2 \neq 0$ have this signal subtracted, and thus image the dynamics of transition charge densities in real space. For points A and B in Fig.(2), the real-space signals show a very different time dependence, because different momenta \mathbf{q}_1 are transferred to the electrons by the first pulse \mathbf{k}_{p1} . The spatial Fourier-transformed real-space signal Eq. (11) is a combination of various (transition) charge densities $\sigma_{ga}(\mathbf{r})$, and can provide information about quantum coherence between the ground and excited states.

IV. DISCUSSION

To compare the LQD signals Eq. (6) with classical diffraction [32] we first note that the former vanishes for a classical field and requires a quantum field. Furthermore, using a light source in which the quantum nature of radiation is prominent, the signal reveals both the amplitude and phase of the charge density. The diffraction can originate from a group of molecules initially in their ground states with a small fraction in the excited state. The relevant material quantity in Eq. (B4) is then $\langle \sigma_{gg} \rangle_\alpha \langle \sigma_{ag} \rangle_\beta$ where α and β represent two molecules, σ_{ag} is a transition charge density (coherence). Classical homodyne diffraction is quadratic in the charge density and originates from pairs of molecules (see Appendix B). The single-molecule contribution, in contrast, originates solely from excited state population since the trace of the diffracted field operators in the expectation value with respect to vacuum state of the field vanishes if the molecule is in a coherent superposition. Classical diffraction carries no information about single molecule coherence.

The multidimensional extension of diffraction imaging with classical light to n diffraction events scales to n -th order in the light *intensity* and $2n$ -th order in the charge density (see Appendix B). The corresponding quantum light signal presented here, in contrast, scales to n -th order in the field *amplitude*. Thus, at a given intensity quantum light allows to observe higher order correlations, thanks to the more favorable intensity scaling. Classical homodyne diffraction dominated by even orders in the charge density is governed by the static (localized) charge density while the new information carried by the phase in the odd contributions provides a novel way of measuring transient charge density, density-density corre-

lations and dynamical events in molecules using quantum diffraction. Generally, the n -th order signals have both amplitude square contributions and lower order phase dependent contributions (such as the ones explored in Fig. (1)). For intense quantum sources with many photons the contribution quadratic in the charge density dominates and the phase dependent terms merely provide a minor correction to the strong background. It is therefore critical to use low photon fluxes in order to isolate the phase-dependent contributions. An alternative way to single out these terms is by employing multiple single photon interferences generated by introducing beam splitters in e.g. Mach-Zehnder interferometers (MZI). The phase of the classical local oscillator field allows to separate real and imaginary part of the material response function and extract the phase in heterodyne measurement. Similar results can be obtained for quantum field by combining the MZI with the phase plates. The multidimensional analogue will be an interesting topic for a future study.

V. ACKNOWLEDGEMENTS

K.E.D. is supported by the Zijiang Endowed Young Scholar Fund and Overseas Expertise Introduction Project for Discipline Innovation (111 Project, B12024). S.M. acknowledges the National Science Foundation (grant CHE-1361516) and the support of the Chemical Sciences, Geosciences, and Biosciences division, Office of Basic Energy Sciences, Office of Science, U.S. Department of Energy through award No. DE-FG02-04ER15571 and de-sc0019484. S.A. was supported by the DOE grant. We wish to thank Noa Asban for the graphical illustrations.

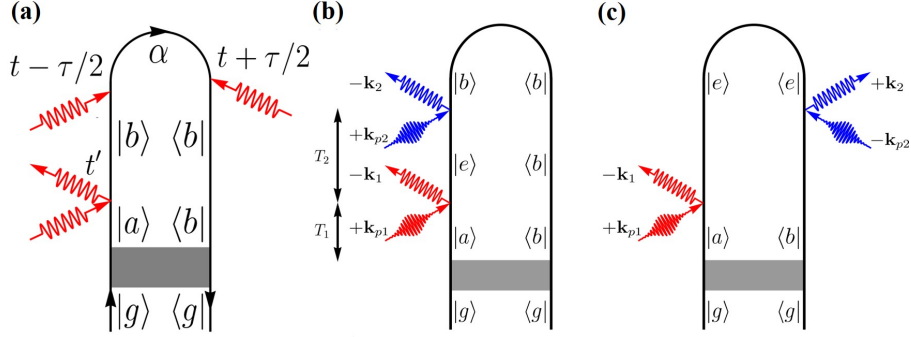


FIG. 5. (a) The loop diagram for the LQD process. An actinic pulse (shaded area) prepares the molecule in a superposition of electronic states ρ_{ab} . After the LQD the state of the system is ρ_{bb} . The top two arrows represent the detection. (b) and (c) The loop diagrams representing the LQD signal in Eq. (7) resulting from two successive scattering measurements. For diagram rules see Ref. [19]

Appendix A: Derivation of the LQD signal

The diffraction pattern is obtained from the time-integrated spatially-gated intensity at point \mathbf{r} of the detector.

$$S_m[\mathbf{q}(\mathbf{r})] = \int dt F_t^I(\bar{t}, t) \times \left\langle \mathcal{T} \mathbf{E}_m^{(-)}(\mathbf{r}, t) \mathbf{E}_m^{(+)}(\mathbf{r}, t) e^{-\frac{i}{\hbar} \int_{-\infty}^t d\tau \mathcal{H}_{I-}(\tau)} \right\rangle, \quad (\text{A1})$$

where m is cartesian component of the field, $\mathbf{q}(\mathbf{r})$ is the diffraction wavevector corresponding to detection at point \mathbf{r} , $F_t^I(\bar{t}, t)$ is a temporal gate, and \mathcal{T} is the time ordering superoperator. \mathcal{H}_{I-} is the interaction superoperator, defined by its action on an ordinary operator X according to $\mathcal{H}_{I-} X \equiv \mathcal{H}_I X - X \mathcal{H}_I$ [33]. By expanding the exponent to first order in \mathcal{H}_{I-} , and separating the incoming (pump) from the detected modes of the electric field we obtain the LQD signal (see Eq. (A2)). For brevity we assume a temporal gating $F_t^I(\bar{t}, t)$ that acts on the intensity, rather than the field (which was $F_t(\bar{t}, t)$). The first order expansion of Eq. (A1) in field-matter interaction yields:

$$S_m^{(1)}(\mathbf{r}) = \frac{2}{\hbar} \Im \int dt F_t^I(\bar{t}, t) \int_{-\infty}^t dt' \int d\mathbf{r}' \langle \sigma(\mathbf{r}', t') \rangle_{\mu} \times \sum_n \langle \psi_p(0) | \mathbf{E}_m^{(-)}(\mathbf{r}, t) \mathbf{A}_n^{(+)}(\mathbf{r}', t') | \psi_p(0) \rangle \langle 0 | \mathbf{E}_m^{(+)}(\mathbf{r}, t) \mathbf{A}_n^{(-)}(\mathbf{r}', t') | 0 \rangle, \quad (\text{A2})$$

where \Im denotes imaginary part, n represents the cartesian coordinates of the vector potential coming from \mathbf{A}^2 interaction term and $\langle \dots \rangle_{\mu} \equiv \text{Tr}[\dots \rho_{\mu}^{(0)}]$ is taken with respect to the initial state of the molecule $\rho_{\mu}^{(0)}$, and $\psi_p(0)$ is the state of the pump photon source.

While the second correlation function over the vacuum state representing detection modes is the same as in the field amplitude signal, the first correlation function over the pump photon state is more peculiar. Assuming the coherent state, the field correlation function reads

$$\langle \psi_p(0) | \mathbf{E}_m^{(-)}(\mathbf{r}, t) \mathbf{A}_n^{(+)}(\mathbf{r}', t') | \psi_p(0) \rangle = \mathcal{E}_m^*(\mathbf{r}, t) \mathcal{A}_n(\mathbf{r}', t'), \quad (\text{A3})$$

where $\mathcal{E}_m(\mathbf{r}, t) = \sum_{\mathbf{k}, \mu} \sqrt{\frac{2\pi\hbar\omega_{\mathbf{k}}}{V_{\mathbf{k}}}} \epsilon_m^{(\mu)}(\mathbf{k}) \alpha_{\mathbf{k}, \mu} e^{i(\mathbf{k}\cdot\mathbf{r} - \omega_{\mathbf{k}}t)}$ and $\mathcal{A}_n(\mathbf{r}, t) = -ic \sum_{\mathbf{k}, \mu} \sqrt{\frac{2\pi\hbar}{\omega_{\mathbf{k}}V_{\mathbf{k}}}} \epsilon_m^{(\mu)}(\mathbf{k}) \alpha_{\mathbf{k}, \mu} e^{i(\mathbf{k}\cdot\mathbf{r} - \omega_{\mathbf{k}}t)}$ with $\alpha_{\mathbf{k}, \mu} = \langle \alpha | \hat{a}_{\mathbf{k}, \mu} | \alpha \rangle$. Note that a similar expression can be achieved for a single photon Fock state $|\psi_{1F}(0)\rangle = \sum_{\mathbf{p}, \lambda} \Phi_{\mathbf{p}, \lambda} |1_{\mathbf{p}, \lambda}\rangle$. In this case the corresponding field amplitudes are given by $\mathcal{E}_m(\mathbf{r}, t) = \sum_{\mathbf{k}, \mu} \sqrt{\frac{2\pi\hbar\omega_{\mathbf{k}}}{V_{\mathbf{k}}}} \epsilon_m^{(\mu)}(\mathbf{k}) \Phi_{\mathbf{k}, \mu} e^{i(\mathbf{k}\cdot\mathbf{r} - \omega_{\mathbf{k}}t)}$ and $\mathcal{A}_n(\mathbf{r}, t) = -ic \sum_{\mathbf{k}, \mu} \sqrt{\frac{2\pi\hbar}{\omega_{\mathbf{k}}V_{\mathbf{k}}}} \epsilon_m^{(\mu)}(\mathbf{k}) \Phi_{\mathbf{k}, \mu} e^{i(\mathbf{k}\cdot\mathbf{r} - \omega_{\mathbf{k}}t)}$ with $\Phi_{\mathbf{k}, \mu} = \langle 0 | \hat{a}_{\mathbf{k}, \mu} | \psi_{1F}(0) \rangle$. Following the method outlined previously and using the following identity:

$$\begin{aligned} & \frac{2\pi\hbar}{V_{\mathbf{k}}} \sum_{\mathbf{k}} \epsilon_m^{(\mu)}(\mathbf{k}) \epsilon_n^{(\mu)}(\mathbf{k}) e^{i\mathbf{k}\cdot\mathbf{R}} \int_{-\infty}^t dt' e^{-i\omega_{\mathbf{k}}(t-t') - i\Omega t'} = \\ & \frac{\hbar}{4\pi} \left[\frac{\Omega^2}{c^2} (\delta_{m,n} - \hat{\mathbf{r}}_m \hat{\mathbf{r}}_n) + \left(\frac{i\Omega}{cR} - \frac{1}{R^2} \right) (\delta_{m,n} - 3\hat{\mathbf{r}}_m \hat{\mathbf{r}}_n) \right] \frac{e^{-i\Omega(t-R/c)}}{\Omega R} \end{aligned} \quad (\text{A4})$$

we obtain for the signal

$$\begin{aligned} S_m^{(1)}(\mathbf{r}) & \propto \Re \int \frac{d\omega'}{2\pi} \sum_{\mathbf{k}, \mathbf{k}_p} \tilde{F}_t^I(\bar{t}, \omega' - \omega_{\mathbf{k}_p} + \omega_{\mathbf{k}}) \langle \sigma(\mathbf{q}_r(\omega'), \omega') \rangle \sum_n \mathcal{E}_m^*(\mathbf{k}) \mathcal{A}_n(\mathbf{k}_p) \\ & \times \left[\frac{\omega_{\mathbf{k}_p} - \omega'}{c} (\delta_{m,n} - \hat{\mathbf{r}}_m \hat{\mathbf{r}}_n) + \frac{i}{r} (\delta_{m,n} - 3\hat{\mathbf{r}}_m \hat{\mathbf{r}}_n) \right] e^{i(\omega_{\mathbf{k}_p} - \omega')r/c - i\mathbf{k}\cdot\mathbf{r}} \end{aligned} \quad (\text{A5})$$

where $\tilde{F}_t^I(\bar{t}, \omega) = \int dt e^{i\omega t} F_t^I(\bar{t}, t)$ is a Fourier transform of the gating function,

$$\mathcal{E}_m^*(\mathbf{k}) = \sum_{\mu} \sqrt{\frac{2\pi\hbar\omega_{\mathbf{k}}}{V_{\mathbf{k}}}} \epsilon_m^{(\mu)}(\mathbf{k}) \chi_{\mathbf{k}, \mu}, \quad (\text{A6})$$

$$\mathcal{A}_n(\mathbf{k}_p) = -ic \sum_{\lambda} \sqrt{\frac{2\pi\hbar}{\omega_{\mathbf{k}_p} V_{\mathbf{k}_p}}} \epsilon_n^{(\lambda)}(\mathbf{k}_p) \chi_{\mathbf{k}_p, \lambda}, \quad (\text{A7})$$

where $\chi = \alpha$ for coherent state and $\chi = \Phi$ for single photon Fock state. Now assuming no temporal gate and taking rotating averaging we obtain Eq. (1).

For the N -photon Fock state the field correlation function Eq. (A3) will contain only same momentum and polarization components of the two fields:

$$\langle \psi_p(0) | \mathbf{E}_m^\dagger(\mathbf{r}, t) \mathbf{A}_{pn}(\mathbf{r}', t') | \psi_p(0) \rangle = \sum_{\mathbf{k}_p, \lambda} \mathcal{E}_{m\lambda}^*(\mathbf{k}_p) \mathcal{A}_{n\lambda}(\mathbf{k}_p) e^{-i[\mathbf{k}_p(\mathbf{r}-\mathbf{r}') - \omega_{\mathbf{k}_p}(t-t)]}, \quad (\text{A8})$$

where

$$\mathcal{E}_{m\lambda}^*(\mathbf{k}_p) = \sqrt{\frac{2\pi\hbar\omega_{\mathbf{k}_p} N_{\mathbf{k}_p, \lambda}}{V_{\mathbf{k}_p}}} \Phi_{\mathbf{k}_p, \lambda}^{(N)*} \epsilon_m^{(\lambda)}(\mathbf{k}_p), \quad (\text{A9})$$

and

$$\mathcal{A}_{n\lambda}(\mathbf{k}_p) = -ic \sqrt{\frac{2\pi\hbar N_{\mathbf{k}_p, \lambda}}{\omega_{\mathbf{k}_p} V_{\mathbf{k}_p}}} \Phi_{\mathbf{k}_p, \lambda}^{(N)} \epsilon_n^{(\lambda)}(\mathbf{k}_p). \quad (\text{A10})$$

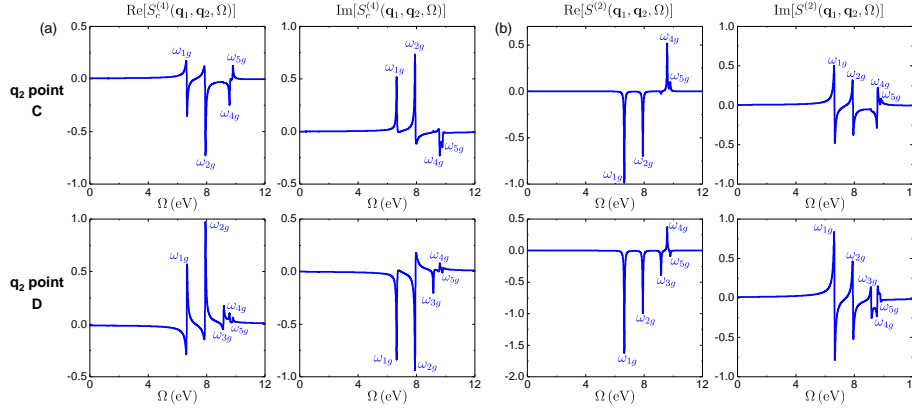


FIG. 6. The real and imaginary parts of signals for (a) classical homodyne $S_c^{(4)}(\mathbf{q}_1, \mathbf{q}_2, \Omega)$ (columns 1 and 2) and (b) LQD $S_q^{(2)}(\mathbf{q}_1, \mathbf{q}_2, \Omega)$ (columns 3 and 4) in frequency domain. The first and second rows show signals at the \mathbf{q}_2 points C and D marked in Fig. 3(a), respectively.

Here we use $\langle \psi_{NF}(0) | \hat{a}_{\mathbf{k}, \nu}^\dagger \hat{a}_{\mathbf{k}_p, \lambda} | \psi_{NF}(0) \rangle = N_{\mathbf{k}_p, \lambda} |\Phi_{\mathbf{k}_p, \lambda}^{(N)}|^2 \delta_{\mathbf{k}, \mathbf{k}_p} \delta_{\nu, \lambda}$. Following the outlined approach the LQD signal yields

$$\begin{aligned}
 S_m^{(1)}(\mathbf{r}) &\propto \Re \int \frac{d\omega'}{2\pi} \sum_{\mathbf{k}_p, \lambda} \tilde{F}_t^I(\bar{t}, \omega') \langle \sigma(\mathbf{q}_r(\omega'), \omega') \rangle \sum_n \mathcal{E}_{m\lambda}^*(\mathbf{k}_p) \mathcal{A}_{n\lambda}(\mathbf{k}_p) \\
 &\times \left[\frac{\omega_{\mathbf{k}_p} - \omega'}{c} (\delta_{m,n} - \hat{\mathbf{r}}_m \hat{\mathbf{r}}_n) + \frac{i}{r} (\delta_{m,n} - 3\hat{\mathbf{r}}_m \hat{\mathbf{r}}_n) \right] e^{i(\omega_{\mathbf{k}_p} - \omega')r/c - i\mathbf{k}_p \cdot \mathbf{r}}, \quad (\text{A11})
 \end{aligned}$$

where $\mathbf{q}(\mathbf{r}) = \mathbf{k}_p + \frac{\omega' - \omega_p}{c} \hat{\mathbf{r}}$. Assuming no temporal gate and taking rotating averaging we simplify the signal to Eq. (4).

The 2D extension of the LQD signal resulting from the two successive scattering measurements is described by the two diagrams of Fig.(5) (and their complex conjugates) stemming from the separation of σ and σ^\dagger that correspond either to both scattering events occur with the ket, or with the ket and the bra (see Fig. 5(b)). The complex conjugate diagrams are not shown. The signal can be read off the diagram and is given by Eq. (7).

Appendix B: Diffraction of classical light

1. Heterodyne detection

A classical heterodyne diffraction is measured by mixing classical diffracted field with another classical local oscillator field. The signal is given by

$$S_c(\mathbf{r}) = \frac{2}{\hbar} \Im \int dt \mathcal{A}_d^*(\mathbf{r}, t) \int dt_1 d\mathbf{r}_1 \mathcal{A}_p(\mathbf{r}_1, t_1) \langle \sigma(\mathbf{r}_1, t_1) \rangle_\mu \quad (\text{B1})$$

This signal is also linear in the charge density. Following the similar derivation presented in Appendix A we obtain for the signal in the CW limit

$$S_c^{(1)}(\mathbf{r}) \propto \Re \mathfrak{e}[\mathcal{A}_d^*(\omega_0)\mathcal{A}_p(\omega_0)\langle\sigma(\mathbf{q}_r(0), 0)\rangle_\mu e^{-i\mathbf{k}_{p'}\cdot\mathbf{r}}]. \quad (\text{B2})$$

2. Homodyne detection

Unlike quantum case and heterodyne classical detection, classical homodyne signal is linear in the field intensity and quadratic in the charge density.

$$S_c^{(2)}(\mathbf{r}) = \frac{2}{\hbar^2} \Re \mathfrak{e} \int dt d\mathbf{r}_1 d\mathbf{r}_1 dt_1 dt_2 \langle\sigma(\mathbf{r}_2, t_2) \sigma(\mathbf{r}_1, t_1)\rangle_\mu \\ \times \langle\mathbf{A}^2(\mathbf{r}_2, t_2) \mathbf{E}^{(-)}(\mathbf{r}, t) \mathbf{E}^{(+)}(\mathbf{r}, t) \mathbf{A}^2(\mathbf{r}_1, t_1)\rangle_\phi. \quad (\text{B3})$$

Following the same steps discussed above the homodyne signal for CW pump is given by

$$S_c^{(2)}(\mathbf{r}) \propto \langle|\sigma(\mathbf{q}_r(0), 0)|^2\rangle_\mu. \quad (\text{B4})$$

Assuming no preparation and time-delayed diffraction denoted by T_1 and expanding the signal Eq. (B4) in sum-over states yields

$$S_c^{(2)}(T_1, \mathbf{q}_1) \propto \langle\sigma^\dagger(T_1, \mathbf{q}_1)\sigma(T_1, \mathbf{q}_1)\rangle = \sum_a |\sigma_{ag}(\mathbf{q}_1)|^2. \quad (\text{B5})$$

3. Multidimensional classical diffraction

The signals studied by Biggs et al. [34] employ contributions linear in the field intensities and are analogous to classical signals which in the impulsive limit read

$$S_c^{(2n)}(\mathbf{q}_1, T_1; \dots; \mathbf{q}_n, T_n) \propto I_1 \dots I_n \\ \times \langle\langle\mathcal{T}\sigma^\dagger(T_1, \mathbf{q}_1)\sigma(T_1, \mathbf{q}_1)\dots\sigma^\dagger(T_n, \mathbf{q}_n)\sigma(T_n, \mathbf{q}_n)\rangle\rangle, \quad (\text{B6})$$

where $I_j = |\mathcal{E}_j|^2$ are field intensities. In Eq. (B6) each diffraction event is quadratic in σ and we omitted the frequency argument in the charge density. Expanding the $n = 2$ signal in sum-over states yields

$$S_c^{(4)}(T_1 = 0, \mathbf{q}_1, T_2, \mathbf{q}_2) \propto \langle\sigma^\dagger(T_1 = 0, \mathbf{q}_1)\sigma^\dagger(T_2, \mathbf{q}_2)\sigma(T_2, \mathbf{q}_2)\sigma(T_1 = 0, \mathbf{q}_1)\rangle \\ = \sum_{ecd} \sigma_{cg}(\mathbf{q}_1)\sigma_{dg}^*(\mathbf{q}_1)\sigma_{ec}(\mathbf{q}_2)\sigma_{ed}^*(\mathbf{q}_2)e^{-i\omega_{cd}T_2}. \quad (\text{B7})$$

Appendix C: The classical homodyne and LQD signals in frequency domain

We select two points C = $(-2.17 \text{ \AA}^{-1}, 0.47 \text{ \AA}^{-1})$ and D = $(0.95 \text{ \AA}^{-1}, -1.42 \text{ \AA}^{-1})$ in Fig. 3(a), and depict the frequency-domain signals in Fig. 6. The peaks at $\Omega = 0$, which correspond to the time-independent pathways and overwhelm other peaks away from the origin ($\Omega = 0$), have been

excluded from Fig. 6. We conclude that the time dependence of the signal is determined by the energy differences between the ground and the excited states.

-
- [1] R. J. Glauber, *Phys. Rev.* **130**, 2529 (1963).
- [2] C.-K. Hong, Z.-Y. Ou, and L. Mandel, *Physical review letters* **59**, 2044 (1987).
- [3] D. Branning, A. L. Migdall, and A. Sergienko, *Physical Review A* **62**, 063808 (2000).
- [4] R. Trotta, J. Martín-Sánchez, J. S. Wildmann, G. Piredda, M. Reindl, C. Schimpf, E. Zallo, S. Stroj, J. Edlinger, and A. Rastelli, *Nature communications* **7**, 10375 (2016).
- [5] D. A. Kalashnikov, A. V. Paterova, S. P. Kulik, and L. A. Krivitsky, *Nature Photonics* **10**, 98 (2016).
- [6] J.-C. Lee and Y.-H. Kim, *Optics Communications* **366**, 442 (2016).
- [7] B. Nordén, *Chemical Physics* **507**, 28 (2018).
- [8] A. V. Paterova, H. Yang, C. An, D. A. Kalashnikov, and L. A. Krivitsky, *Quantum Science and Technology* **3**, 025008 (2018).
- [9] F. Krausz and M. Ivanov, *Reviews of Modern Physics* **81**, 163 (2009).
- [10] T. Ishikawa, H. Aoyagi, T. Asaka, Y. Asano, N. Azumi, T. Bizen, H. Ego, K. Fukami, T. Fukui, Y. Furukawa, *et al.*, *nature photonics* **6**, 540 (2012).
- [11] S. Corde, K. T. Phuoc, G. Lambert, R. Fitour, V. Malka, A. Rousse, A. Beck, and E. Lefebvre, *Reviews of Modern Physics* **85**, 1 (2013).
- [12] M. Chini, K. Zhao, and Z. Chang, *Nature Photonics* **8**, 178 (2014).
- [13] C. Bostedt, S. Boutet, D. M. Fritz, Z. Huang, H. J. Lee, H. T. Lemke, A. Robert, W. F. Schlotter, J. J. Turner, and G. J. Williams, *Reviews of Modern Physics* **88**, 015007 (2016).
- [14] A. E. Cohen and S. Mukamel, *Phys. Rev. Lett.* **91**, 233202 (2003).
- [15] S. Mukamel and K. E. Dorfman, *Phys. Rev. A* **91**, 053844 (2015).
- [16] J. Miao, P. Charalambous, J. Kirz, and D. Sayre, *Nature* **400**, 342 (1999).
- [17] J. Miao, T. Ishikawa, E. H. Anderson, and K. O. Hodgson, *Phys. Rev. B* **67**, 174104 (2003).
- [18] J. R. Rouxel, M. Kowalewski, K. Bennett, and S. Mukamel, *Phys. Rev. Lett.* **120**, 243902 (2018).
- [19] C. A. Marx, U. Harbola, and S. Mukamel, *Physical Review A* **77**, 022110 (2008).
- [20] A. M. Maiden and J. M. Rodenburg, *Ultramicroscopy* **109**, 1256 (2009).
- [21] E. Candès, Y. Eldar, T. Strohmer, and V. Voroninski, *SIAM Review* **57**, 225 (2015), <https://doi.org/10.1137/151005099>.
- [22] S. Asban, K. E. Dorfman, and S. Mukamel, (2018).
- [23] K. Bennett, J. D. Biggs, Y. Zhang, K. E. Dorfman, and S. Mukamel, *J. Chem. Phys.* **140**, 204311 (2014), <https://doi.org/10.1063/1.4878377>.
- [24] S. Tanaka, V. Chernyak, and S. Mukamel, *Phys. Rev. A* **63**, 063405 (2001).
- [25] V. Y. Chernyak, P. Saurabh, and S. Mukamel, *J. Chem. Phys.* **143**, 164107 (2015).
- [26] S. Mukamel and H. J. Bakker, *J. Chem. Phys.* **142**, 212101.
- [27] H. Werner, P. Knowles, G. Knizia, F. Manby, M. Schütz, P. Celani, T. Korona, R. Lindh, A. Mitrushenkov, G. Rauhut, *et al.*, see <http://www.molpro.net> (2010).
- [28] T. H. Dunning Jr, *J. Chem. Phys.* **90**, 1007 (1989).
- [29] H.-J. Werner and W. Meyer, *J. Chem. Phys.* **73**, 2342 (1980).
- [30] H.-J. Werner and P. J. Knowles, *J. Chem. Phys.* **82**, 5053 (1985).
- [31] P. J. Knowles and H.-J. Werner, *Chem. Phys. Lett.* **115**, 259 (1985).
- [32] M. Kowalewski, K. Bennett, and S. Mukamel, *Structural Dynamics* **4**, 054101 (2017), <https://doi.org/10.1063/1.4984241>.
- [33] U. Harbola and S. Mukamel, *Phys. Rep.* **465**, 191 (2008).
- [34] J. D. Biggs, K. Bennett, Y. Zhang, and S. Mukamel, *J. Phys. B: At. Mol. Opt. Phys.* **47**, 124037 (2014).